Journal of Alloys and Compounds 746 (2018) 509–519

Contents lists available at ScienceDirect

Journal of Alloys and Compounds

journal homepage: http://www.elsevier.com/locate/jalcom

Cyclic oxidation characteristics of HVOF thermal-sprayed NiCoCrAlY and CoNiCrAlY coatings at 1000 °C

A. Feizabadi [a], M. Salehi Doolabi [b], S.K. Sadrnezhaad [b, *], M. Rezaei [c]

[a] Department of Chemistry, The University of Western Ontario, London, Ontario, N6A 5B7, Canada
[b] Department of Materials Science and Engineering, Sharif University of Technology, Azadi Ave., P.O. Bo11365-9466, Tehran, Iran
[c] Department of Mining and Metallurgical Engineering, Amirkabir University of Technology, P.O. Box: 15875-4413, Tehran, Iran

ARTICLE INFO

Article history:
Received 30 December 2017
Received in revised form
20 February 2018
Accepted 22 February 2018
Available online 23 February 2018

Keywords:
MCrAlY coatings
High velocity oxygen and fuel
Cyclic oxidation
Thermally grown oxide

ABSTRACT

Thermal-sprayed MCrAlY coatings have become widespread in various industries such as power plants, aeronautics, and oil and gas firms. High-temperature oxidation behavior of these coatings is therefore of significance. Spraying of two prevalent MCrAlY powders (NiCoCrAlY and CoNiCrAlY) on Hastelloy substrate by high velocity oxygen and fuel method and exposing them to 1000 °C air for resolving of their cyclic oxidation behavior are presented in this paper. The coatings were characterized by x-ray diffraction, scanning electron microscopy and energy-dispersive x-ray spectroscopy. The obtained oxidation kinetic indicated that at 1000 °C, the thermally sprayed NiCoCrAlY coating has greater resistance to oxidation than CoNiCrAlY. While oxidation rate of the former follows a parabolic rate equation with specific rate of 5.1×10^{-3} $(\mu m)^2 h^{-1}$ at 1000 °C, the oxidation rate for the latter has a specific rate of 12.1×10^{-3} $(\mu m)^2 h^{-1}$.

1. Introduction

Progress in turbine technology requires highly developed coatings with qualified specifications such as resistance to diverse aggressive environments, consistent coating-substrate thermal expansion and prolonged resource of the advantageous elements like Al and Cr [1,2]. Simultaneous meeting of these demands is arduous for overlay coatings. After so many attempts for improvement of the efficiency of various coatings, MCrAlY (M = Ni, Co, or both) has been announced as the fitting case [3]; capable of forming (a) Al-rich layer resistant to type 1 hot corrosion and (b) Cr-rich layer highly resistant to type 2 hot corrosion [4].

MCrAlY coatings have widely been used in gas turbine engines as (a) overlay protective layer and (b) bond coat for Thermal Barrier Coatings (TBCs) [3–5]. Al plays a vital role in these coatings because its selective oxidation produces a continuous, compact and stable Al_2O_3-rich scale on the surface of the layer. Diffusion of oxygen through Al_2O_3 is slow; so the protective oxide scale gradually thickens with least stress exertion [4,6]. Another vital element in MCrAlY is Yttrium which can enhance the protective scale adhesion to the coating [7,8].

There are diverse thermal spraying methods to implement MCrAlY overlay coatings on the substrates such as Vacuum Plasma Spraying (VPS), High Velocity of Oxygen and Fuel (HVOF), Atmospheric Plasma Spraying (APS) and Low-Pressure Plasma Spraying (LPPS) [9]. As the cost of under-vacuum operation is high, other techniques have gotten more usage [10]. Recent researches have proved that the High Velocity Oxygen and Fuel (HVOF) coatings have better property in comparison to the other methods because HVOF can form an Al_2O_3 dispersion on the surface during the coating process [11–13]. It has been proved that the efficiency of the overlay coatings not only depends on the used thermal spraying method but also on the chemical composition of the coating [14–16].

In this study, NiCoCrAlY and CoNiCrAlY are first coated on Hastelloy samples by HVOF method. Oxidation behaviors of both coatings are then studied and compared with each other and with a bare Hastelloy sample. Rate equations for oxidation of the coatings are determined and possible prevailing mechanisms are suggested. Due to long-term dominance of ~1000 °C in most turbine blade parts and their exposure to cyclic condition, cyclic oxidation studies are carried out at 1273 K.

* Corresponding author.
E-mail address: sadrnezh@sharif.edu (S.K. Sadrnezhaad).

https://doi.org/10.1016/j.jallcom.2018.02.282
0925-8388/

2. Materials and methods

2.1. Materials

Gas Atomized NiCoCrAlY and CoNiCrAlY powders (made of Metco Com., USA) of spheroidal morphology and 20–45 and 5.5–38 μm respective diameters and nominal chemical compositions given in Table 1 were used as coating feedstock. The nominal chemical composition of the Hastelloy substrate is also listed in Table 1.

2.2. Coating

Prior to spraying the powders, the Hastelloy sheets were grit blasted using alumina powder to increase the adherence of the coating to the substrate. Then we cleaned the substrate by using acetone ultra-sonication. Both sides of the sheets were entirely sprayed with MJ500 (Sulzer-Metco) gun and KR16 robot (KUKA, Germany) which used kerosene as fuel and nitrogen as carrier gas for accomplishment of the HVOF process. The approximate thickness of the final coating was 200 ± 20 μm. During and after the spray, air jets cooled down the surfaces of the samples. When both surfaces were totally coated, we cut the substrate into $20 \times 10 \times 2$ mm specimens. Table 2 summarizes the working parameters used to coat the Hastelloy samples.

2.3. Oxidation

We oxidized all samples at 1000 °C with air at a heating rate of 20 °C/min via either 4 or 8 heating cycles which took 20 h, each. After every cycle, we took the sample out of the furnace and cooled it down to the room temperature, which took ~30 min and measured its weight by an electronic balance of 10^{-4} g precision and its TGO thickness using Scanning Electron Microscope (SEM).

2.4. Analysis

Scanning Electron Microscope (SEM) (Hitachi, Japan; Model: S-3400N) equipped with EDS microanalysis unit revealed microstructure, surface morphology and chemical composition of the coatings. X-ray diffraction (XRD, Model D/Max 2500PCRigaku, Japan: Cu Kα radiation) asserted composition and phase analysis of the coatings. To maintain the surface oxide layer, samples were Nickel plated before metallographic preparation.

3. Result and discussion

Figs. 1 and 2 show the XRD results of the as-coated samples. While the major phase in both sprayed coatings is γ/γ ', an important difference between the two samples is stronger peaks of the main β phase in NiCoCrAlY as compared with the CoNiCrAlY coating. This β phase is more stable and resistant to high temperature oxidation than most other phases of both samples (except Al_2O_3), as indicated by previous authors [7,11,17]. Exposing both coatings to high temperature (i.e. 1000 °C) reveals higher oxidation resistance of NiCoCrAlY than CoNiCrAlY. Experimental results have displayed the former as the owner of the highest thermal efficiency.

Table 1
Nominal chemical composition of the materials used in this research.

Material	Constituents (wt%)								
	Ni	Co	Cr	Al	Y	Fe	Mo	C	W
NiCoCrAlY	Bal.	23.0	17.0	12.5	0.45	–	–	–	–
CoNiCrAlY	32.0	Bal.	21.0	8.0	0.45	–	–	–	–
Hastelloy	Bal.	1.5	22.0	2.0	–	15.8	9.0	0.15	0.6

Table 2
HVOF process parameters.

Parameter	Value
Spray distance, mm	320
Powder feed rate, g/min	50
N_2 carrier gas flow rate, L/min	5
O_2 gas flow rate, L/min	820
Kerosene flow rate, mL/min	360
Speed of robot, mm/s	500

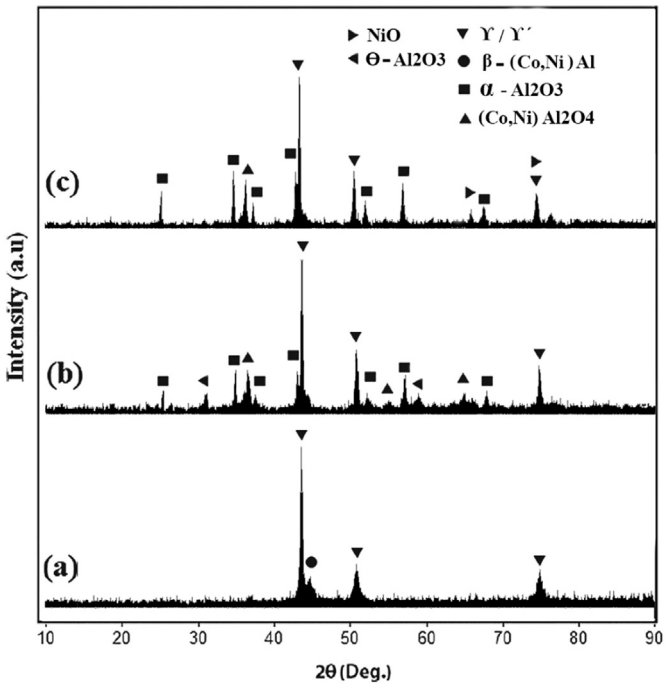

Fig. 1. XRD patterns of the CoNiCrAlY coating: (a) as-coated, (b) after 80 h oxidation and (c) after 160 h oxidation.

Figs. 1 and 2 also show the formation of α-alumina after 80 h oxidation on both NiCoCrAlY and CoNiCrAlY coatings. Due to the higher density and uniformity of α-alumina protective layer in comparison to the other generated layers on the surface of the coating, it has been referred to as the main protective layer on the surface of the specimens [18,19]. Other detected oxides like $NiAl_2O_4$ and $CoAl_2O_4$ spinels have not been as beneficial as the α-alumina phase; because of their reduction of resistance to oxidation [20]. By increasing the oxidation time from 80 to 160 h, NiO, another detrimental phase, may appear in the CoNiCrAlY coating. This phase severely reduces the lifetime of the coating, according to the literature [21]. It uses much higher depth of the coating to be generated while acting as nucleation site for creation of crack [22].

Let's divide both coatings into the following three zones shown in Fig. 3:

1 Outer-β-depleted zone (OBDZ)
2 β-left zone (BLZ)
3 Inner-β-depleted zone (IBDZ)

Fig. 3 depicts the mechanism of formation of Al_2O_3 by high temperature oxidation of the coatings. The first step is the formation of a protective aluminum oxide layer on the oxide-less surface

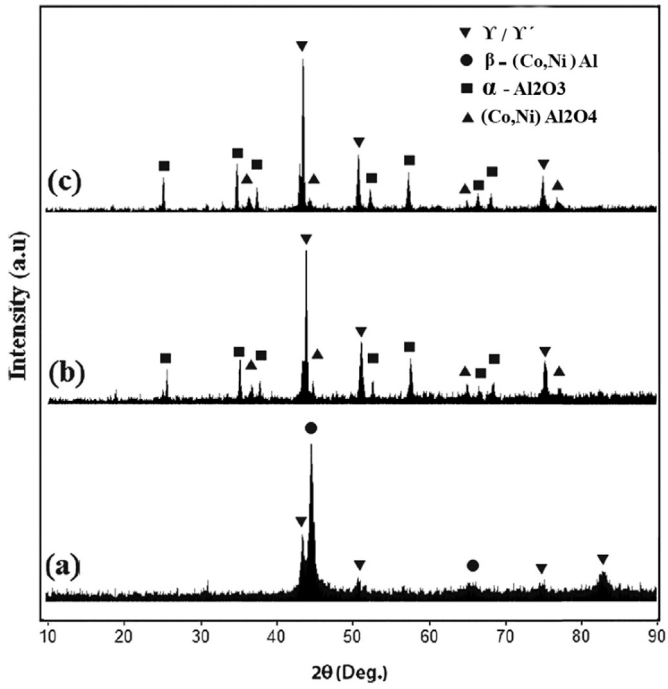

Fig. 2. XRD patterns of the NiCoCrAlY coating: (a) as coated, (b) after 80 h oxidation and (c) after 160 h oxidation.

of the sample. This is due to lower Gibbs free energy of formation of Al_2O_3 at 1000 °C than other possible oxides [21]. Diffusion of aluminum from the β phase of the coating results in thickening of the protective alumina layer (OBDZ) [23]. Large difference between the Al concentration of the coating and the substrate leads to diffusion of Al from the coating to the substrate, which makes the IBDZ thick.

Sufficient Al in the β phase can provide adequate aluminum for formation of uniform alumina layers in both CoNiCrAlY and NiCoCrAlY coatings. Produced alumina layer can act as an obstacle to inward and outward diffusion of oxygen anions and metal cations. As is displayed in Fig. 3, before the formation of spinel oxides, the predominant oxidation mechanism is diffusion of cations towards the interface. After formation of the spinel, simultaneous diffusion of anions and cations within the defect-full permeable oxide layer is the prevailing mechanism according to the literature [4]. Anions diffusion causes the sub-scale alumina formation underneath the thermally grown oxide (TGO) phase, too [24].

Problem arises when β phase does not have enough aluminum to support the generation of the protective layer. Minimum aluminum content for re-healing the alumina layer is 3 percent, according to the previous researches [25].

Selective oxidation of Al, depletes close-to-surface β phase of the coating. By lowering of the β phase to a specified critical level, other elements such as Ni, Cr and Co can diffuse through defects of the alumina phase towards the surface [23]. These elements may then begin to oxidize to cause nucleation of spinel-oxides on the surface. Fast growth of these spinels will increase the oxidation rate of the coatings at the surface and since the spinel oxides are more permeable and less spallation resistant than the alumina phase, formation of any mixture containing alumina together with spinel oxides reduces resistance to high temperature oxidation, too.

Plotting the thermodynamic stability diagram of Ni-Al-O system can be so beneficial due to its description about the equilibrium between different phases that can be generated in this system. This diagram can be provided utilizing the standard free energies of formation of phases at 1000 °C. The obtained diagram is presented in Fig. 4 and all the equilibriums presented in this diagram are as follows:

$$2Al + \frac{3}{2}O_2 = Al_2O_3 \quad (1.1)$$

$$Ni + 2Al + 2O_2 = NiAl_2O_4 \quad (1.2)$$

$$Ni + \frac{1}{2}O_2 = NiO \quad (1.3)$$

$$3Ni + 4Al_2O_3 = 3NiAl_2O_4 + 2Al \quad (1.4)$$

$$NiAl_2O_4 + 3Ni = 4NiO + 2Al \quad (1.5)$$

In the present system, although oxygen pressure at the surface is enough for formation of the spinel oxide phases, it is not as much in the depth to change exclusivity of the alumina layer. On the other hand, a_{Al} is minimum at the surface and will have its maximum amount at the bulk. Using the mentioned information and the thermodynamic stability diagram can justify the cause for formation of the duplex oxide layer on the surface as shown in Figs. 5 and 6.

According to Fig. 2, the spinel oxide peaks of the CoNiCrAlY

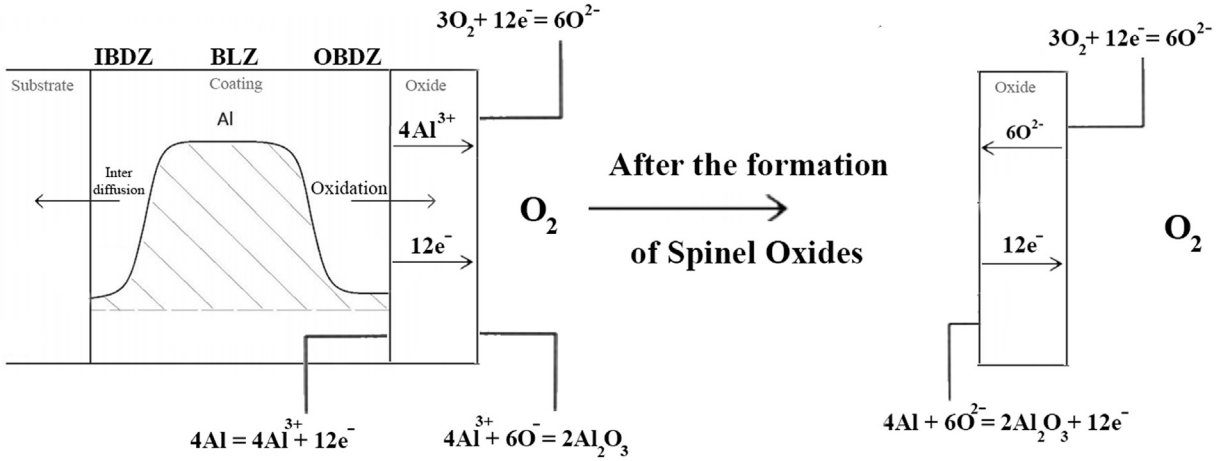

Fig. 3. Mechanism of oxidation of Al before and after formation of spinel oxides.

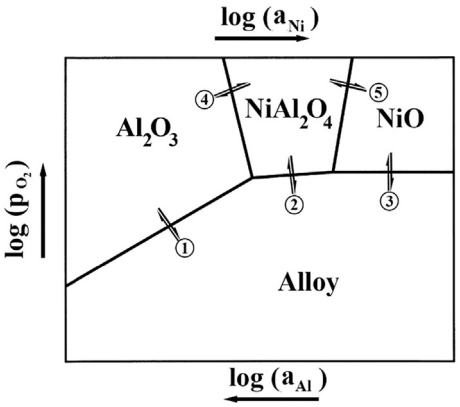

Fig. 4. The thermodynamic stability diagram of Ni-Al-O system.

coating after 160 h oxidation is stronger than 80 h. This change suggests increasing of the thickness of the spinel oxide layer by oxidation time. Fig. 5 compares the SEM cross-sectional images of the CoNiCrAlY coating after 80 and 160 h oxidation. The figure approves the thickening of the spinel oxide layer by oxidation duration.

Unlike CoNiCrAlY coating, NiCoCrAlY layer demonstrates much higher resistance to oxidation. Spinel oxides are not as predominant as alumina layer on the surface of the NiCoCrAlY coating. This indicates that the NiCoCrAlY coating does not totally deplete from β phase in its depth even after 160 h oxidation. For these reasons, the NiCoCrAlY coating shows higher resistance, greater service-life and lower k_p than CoNiCrAlY coating, as will be discussed in the coming sections.

SEM images shown in Figs. 5 and 6 are also of help to recognize the much higher resistance of NiCoCrAlY layer to oxidation than CoNiCrAlY coating. Comparison of the images shows that 80 h oxidation of CoNiCrAlY forms a dense and uniform oxide layer much thicker than that of NiCoCrAlY. Although higher diffusion rate of aluminum in the first stage of oxidation of CoNiCrAlY coating can be advantageous, long time exposure of the coating to high temperature may cause detrimental effects due to depletion of the aluminum reserve in CoNiCrAlY. This depletion can decrease the a_{Al} in CoNiCrAlY coating and as it is visible in the thermodynamic stability diagram in Fig. 4, it can prepare the situation for generation of spinel oxides. As the TGO layer is growing much faster in the CoNiCrAlY coating it can be derived that the aluminum diffuse with higher rate in this coating than the NiCoCrAlY. So the β depleted zone in the coating-oxide interface is much thicker in the CoNiCrAlY coating than the other. Fig. 6 shows that by increasing the oxidation time, TGO will become thicker and thicker. That may generate tensile stress in the coating, as indicated by previous authors [26,27]. The generated stress can cause spallation and loss of TGO uniformity as shown in Fig. 7 and this will result in service-life reduction. From greater life time of NiCoCrAlY, it is deduced that TGO of NiCoCrAlY is more resistant to diffusion than CoNiCrAlY. Lower diffusion rate of elements in NiCoCrAlY reduces the growth rate of TGO and this will lead to smaller Al assumption from the β Al reservoir which results in higher resistance to oxidation.

As is visible in Fig. 7, devastation of some areas of the protective layer on CoNiCrAlY, partly exposes the sample to the oxidizing hot atmosphere. The TGO layer of NiCoCrAlY coating of Fig. 7 is, however, free of any spallation and the dual-layer oxide (Spinel oxide and α-Alumina containing outer and inner layers) seems continuous and uniform.

As can be seen in Fig. 7, roughness of both coatings have increased by time of oxidation; but CoNiCrAlY is much rougher. The average surface roughness (Ra) of the coatings measured after 160 h oxidation using the Mitutuyo SJ-210 surface roughness tester was 4.6 μm for NiCoCrAlY and 5.5 μm for CoNiCrAlY. Since the failure of the coating can start from the surface, intense roughness of CoNiCrAlY can be an indication of its low resistance to spallation.

The elemental concentration profile of both coatings before and after 160 h oxidation are presented in Figs. 8 and 9. The data proves our previous claim about less Al consumption in the case of NiCoCrAlY coating. As can be seen in Figs. 8 and 9, the concentrations of Co, Ni and Cr are higher on the surface of CoNiCrAlY after 160 h oxidation (Due to the higher lattice parameter of θ-Alumina in comparison to the α-Alumina) than NiCoCrAlY. The Al in-depth reservoir of CoNiCrAlY is, hence, much lower than NiCoCrAlY after 160 h oxidation.

SEM images taken from the surfaces of both coatings after 160 h oxidation are presented in Fig. 10. More cracks are observable on CoNiCrAlY than NiCoCrAlY which confirms lower protection potency of the former. The reason for the higher crack density of CoNiCrAlY is to be discussed further.

From XRD results, it is deduced that prolonged oxidation of the samples results in the conversion of the β-BCC phase (with 0.286 nm lattice parameter) into γ-FCC phase (with 0.354 nm lattice parameter) due to the Al depletion which results in straining of the coated layer [28,29]. The CoNiCrAlY coating that endures faster β to γ transformation will experience much higher strain induction

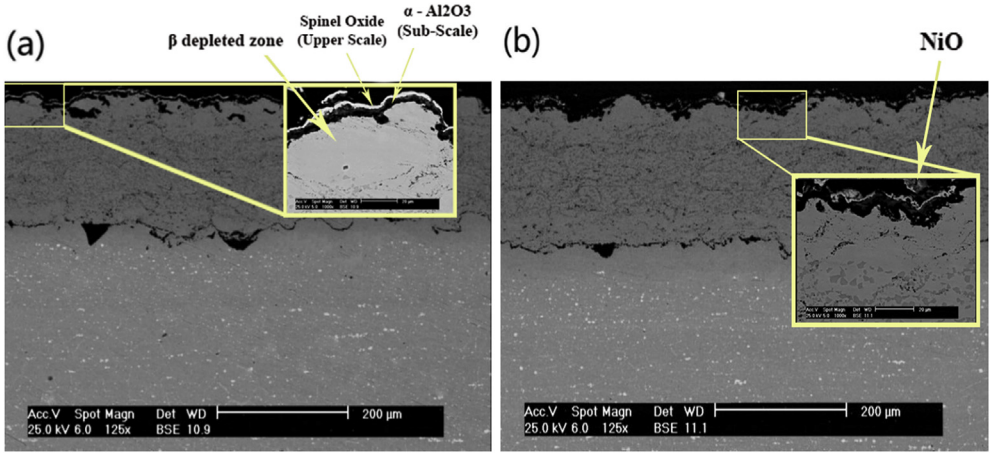

Fig. 5. Cross-sectional representation of the SEM image showing CoNiCrAlY coating after: (a) 80 h and (b) 160 h high-temperature oxidation.

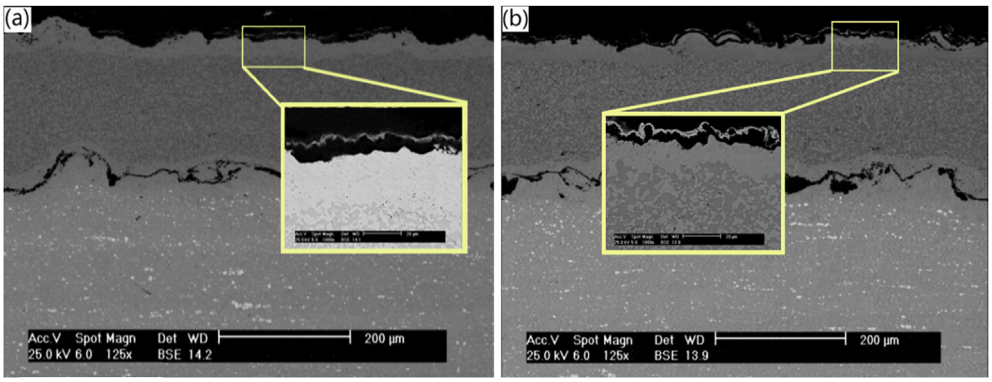

Fig. 6. Cross-sectional representation of the SEM image showing NiCoCrAlY coating after: (a) 80 h and (b) 160 h oxidation.

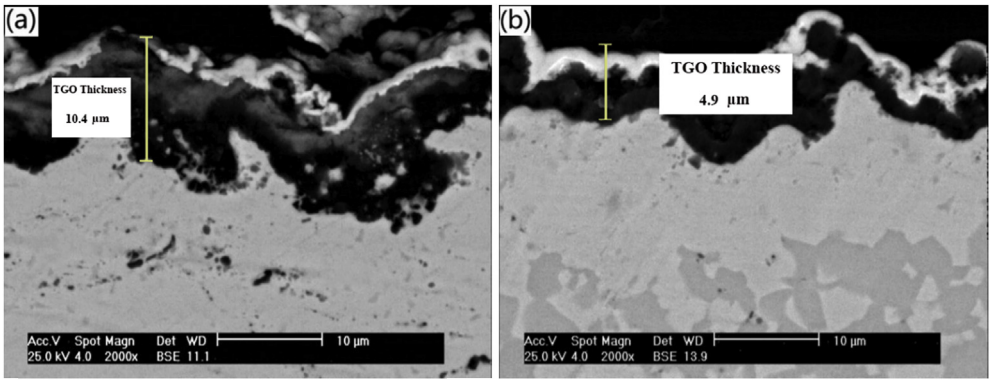

Fig. 7. Cross-sectional SEM images of the coatings after 160 h oxidation: (a) CoNiCrAlY and (b) NiCoCrAlY. Average TGO thickness is tagged in the figure.

and crack initiation than NiCoCrAlY, as also reported by previous researchers [30].

Formation of θ-Alumina in the first stage of oxidation on the CoNiCrAlY is another reason for its low protection strength. After 160 h oxidation, the quantity of this phase is too low to be detectable by XRD test. Its needle-like shape is, however, recognizable in Figs. 10(a) and 11(a). Monoclinic θ-Alumina has ~12 percent lower density than rhombohedral α-Al_2O_3 and its transformation to the lower lattice phase after long time exposure to high oxidizing temperature contracts the volume and imposes high stress to the coating which facilitates crack formation [31,32]. As it is visible in Fig. 11, the surface of the CoNiCrAlY coating after 80 h oxidation is partly covered with needle-like θ-Alumina which is almost crack-free. However, it is shown in Fig. 10 that after 160 h oxidation most θ-Alumina has transformed to crack covered α-Alumina phase. The main reason that the θ-Alumina transient phase is more prevalent on the surface of CoNiCrAlY coating can, hence, be referred to the grain boundary effects of β-NiAl. Yang et al. [33], have found that the α-Alumina will nucleate at the grain boundaries of β-NiAl phase. The grain size of this phase in both coatings before high temperature oxidation test are calculated from the well-known Scherrer equation:

$$t = \frac{0.9\lambda}{B\cos\theta_B} \tag{2}$$

where t is the mean size of the grains, λ is the X-ray wavelength, β is the line broadening at half peak intensity and θ is the Bragg angle [34].

The calculated grain size of the β-NiAl phase of NiCoCrAlY and CoNiCrAlY coatings are 11 and 16 nm, respectively. So, it is clear that the NiCoCrAlY coating has a higher specific grain-boundary than CoNiCrAlY coating which can act as nucleation site for the α-Alumina phase. On the other hand it was discussed before in the XRD results that the stronger peaks of β-NiAl in NiCoCrAlY coating can be referred to the higher density of this phase in this coating, so that's why, the proper locations for the nucleation of α-Alumina phase in the CoNiCrAlY coating is lower in comparison to the other coating.

To draw a better perspective of the matter, we use the Pilling-Bedworth ratio, as explained below [35]:

$$PBR = \frac{V_{oox}}{V_{om}} \tag{3}$$

where PBR is Pilling-Bedworth Ratio, V_{oox} is volume of the oxide formed and V_{om} is volume of metal consumed to form the oxide layer.

As it is known from the previous studies, oxides of most metals have higher volume than the utilized metal with PBR>1. This creates a compressive coating stress. But in some cases, such as the transformation of the θ-Alumina to α-Al_2O_3, tensile stress is created by utilization of θ-Alumina which have higher volume than α-Al_2O_3 and PBR being less than 1. The progressive increase in tensile stress

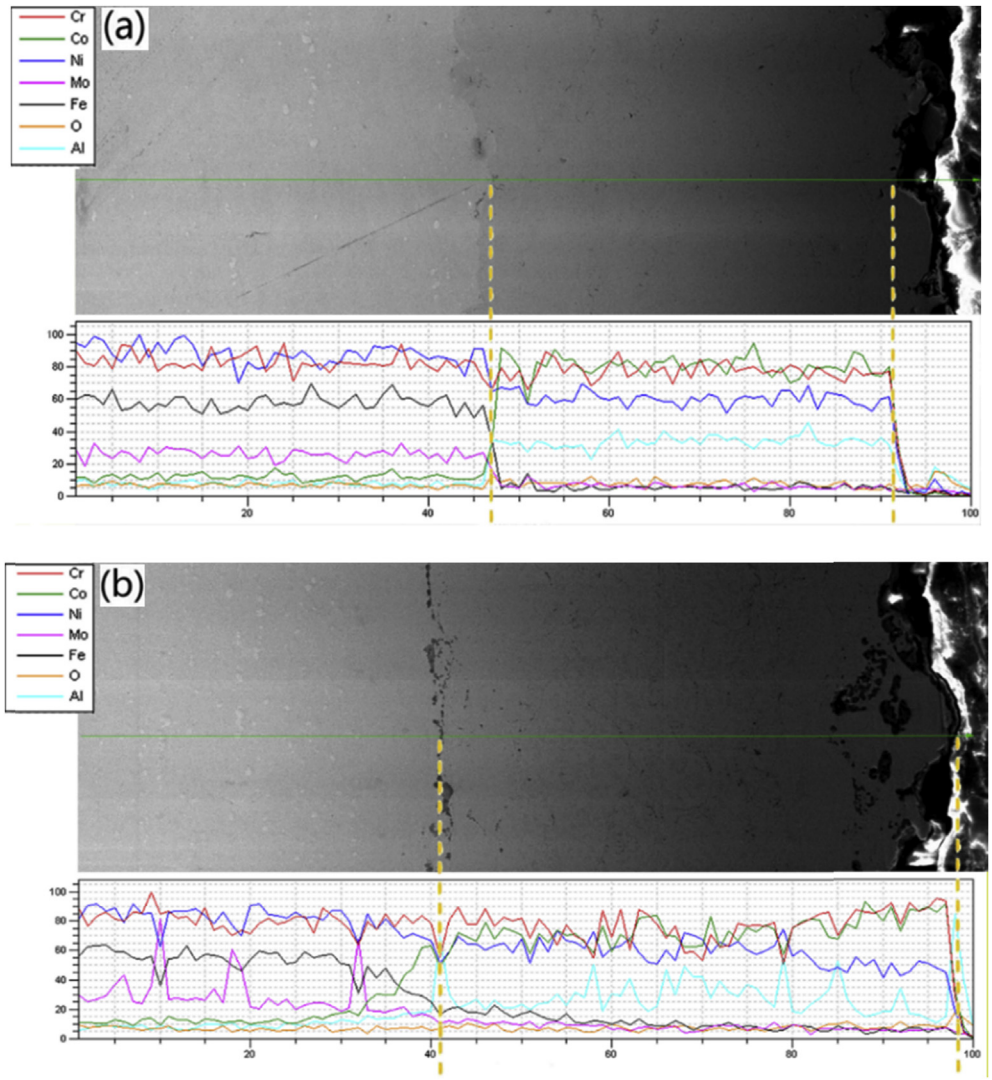

Fig. 8. Elemental concentration profiles across the thickness of CoNiCrAlY: (a) as coated and (b) after 160 h.

will enhance the oxide growth rate, as was seen in our experiments. So the tensile stress and other mentioned reasons, make the oxide growth rate much higher in CoNiCrAlY than the other implemented coating [26]. Transformation of θ-Alumina to α-Al_2O_3 can make some defects that increase the nucleation of cracks, too.

It is necessary that the generated phases on the coatings make uniform, thick and well-adhered layer on the surface to protect the coating and substrate under the service temperature. But in most cases, the large difference between thermal expansion coefficients of the generated phases can impose high strain to the coating that can result in creation of large stresses which cause crack initiation [26,36].

The strain energy produced in the coating-oxide interface upon cooling of the specimen can be calculated from Equation (4) [37]:

$$W^* = E_{ox}h(1 - V_{ox})(\Delta T)^2(\Delta\alpha) \quad (4)$$

where W^* is the strain energy, E_{ox} is Young's Modulus of the oxide, h is the oxide thickness, V_{ox} is Poisson's ratio of the oxide, ΔT is change in the temperature and Δα is the difference in the thermal expansion coefficients.

As it is visible in Equation (4), the thickness and the difference between the thermal expansion coefficients (CTE) are the distinct parameters of the oxides generated in the coating. CTE for θ-Alumina is 7.0×10^{-6}, for α-Al_2O_3 is 8.5×10^{-6} and for CoNiCrAlY and NiCoCrAlY both are approximately the same (~18.4×10^{-4}). The difference between the thermal expansion coefficients of the formed θ-alumina and CoNiCrAlY coating causes much higher strain in the coating which will lead to stresses on the coating. While these generated stresses exceed the fracture energy of the Alumina on Ni substrate, which is 0.66 Jm^{-2}, cracks will be created [38,39].

As can be seen in Fig. 10(b), although NiCoCrAlY coating has much higher resistance to cracking and spallation, some visible cracks still exists on the coating surfaces. The most logical reason for generation of these cracks is high density of β phase in NiCoCrAlY after 160 h oxidation. As it was mentioned before there are diverse sources of stress and crack initiation on coating surfaces such as conformational changes in the β phase [40]. In the oxidation process, the β phase having B2 structure will change to $L1_0$ martensite upon cooling which imposes high stress on the coating due to its ~2% volume contraction. This can cause crack nucleation

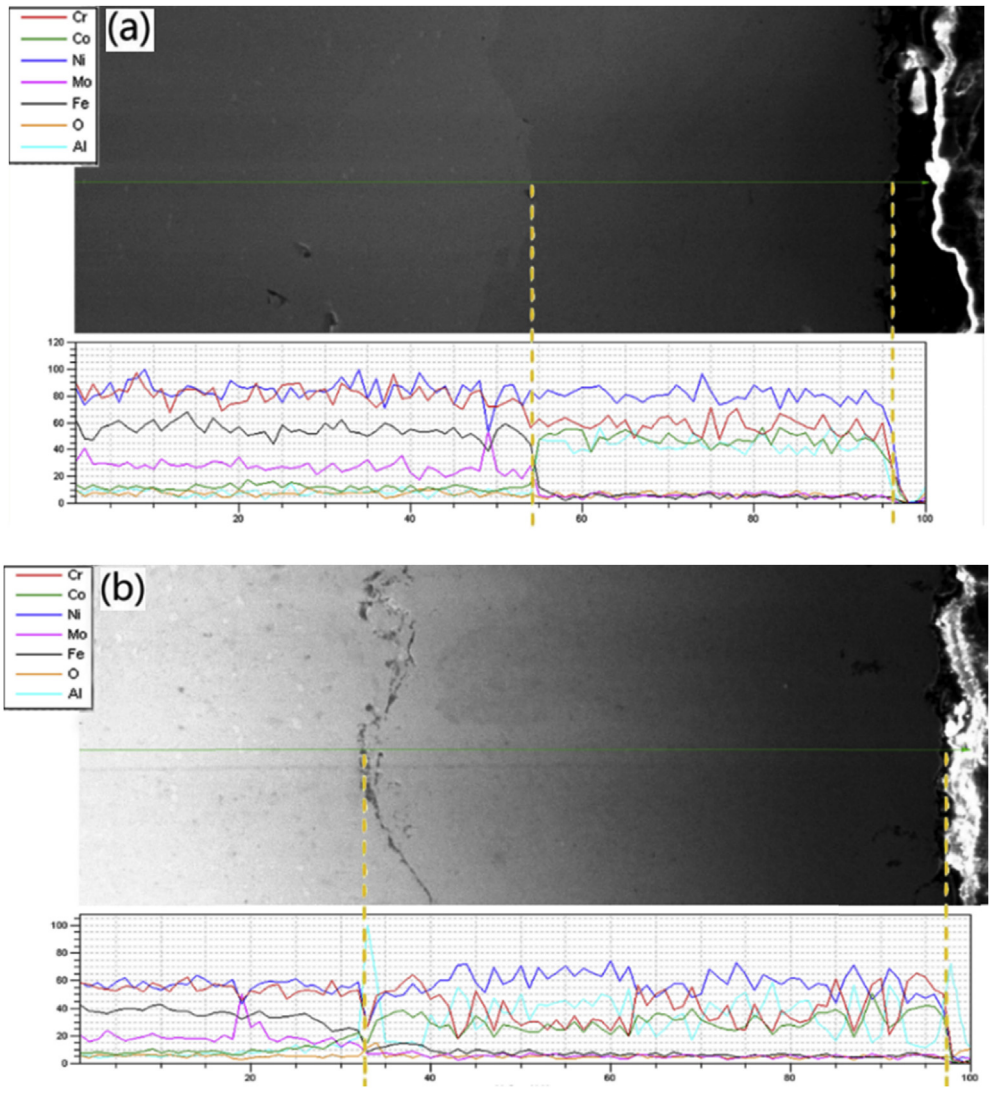

Fig. 9. Elemental concentration profiles across the thickness of NiCoCrAlY: (a) as coated and (b) after 160 h oxidation.

on the surface of the coating. This transformation can be the principal reason for the observed cracks on the NiCoCrAlY coating.

To obtain better perspective of difference between the produced coatings, we studied kinetics of oxidation of the samples [41]. Parabolic rate law have shown best fitting by previous researchers [28,42]. We used both TGO thickness and specific weight change of the samples for determination of the kinetic parameters. The experimental results were plotted against the oxidation time for NiCoCrAlY and CoNiCrAlY, as indicated in Fig. 12. Using TGO thickness data showed prevalence of a parabolic regime (Equation (5)), with different rate constants for different coatings:

$$\delta^2 = 2.k_p^{/}.t \tag{5}$$

Rate constants obtained from the TGO thickness data were 0.0051 and 0.0121 $(\mu m)^2\,h^{-1}$ for NiCoCrAlY and CoNiCrAlY, respectively. It was concluded that at the same oxidation temperature, the CoNiCrAlY coating has higher oxidation rate than NiCoCrAlY which seems to be the ideal coating in oxidation system of this research.

In an alternative evaluation procedure similar to that of previous authors [43,44], squared specific mass-change was plotted against the oxidation time (Fig. 13). The curve obtained for NiCoCrAlY was semi-linear indicating prevalence of the parabolic law (Equation (6)) with a rate constant value of 6.2×10^{-3} $(mg\,cm^{-2})^2\,h^{-1}$:

$$\left(\frac{\Delta m}{A}\right)^2 = k_p.t \tag{6}$$

Unlike NiCoCrAlY, curve fitting for the CoNiCrAlY coating showed sub-parabolic behavior expressed by Wagner Equation (7):

$$\left(\frac{\Delta m}{A}\right)^n = k_p.t \tag{7}$$

Rate constants of the first regime (before 80 h) was 1.7×10^{-2} $(mg\,cm^{-2})^{2.5}.h^{-1}$ (with the growing exponent of n = 2.5) and 14.6×10^{-3} $(mg\,cm^{-2})^2\,h^{-1}$ (after 80 h). Higher weight-gain rate of CoNiCrAlY in the first stage of oxidation seemed due to θ-Alumina and heavier spinel oxides formation. Unlike CoNiCrAlY, the NiCoCrAlY coating showed much higher resistance to the formation of spinel and other unwanted oxides and the principal resource of the mass gain was the generation of the α-Alumina layer.

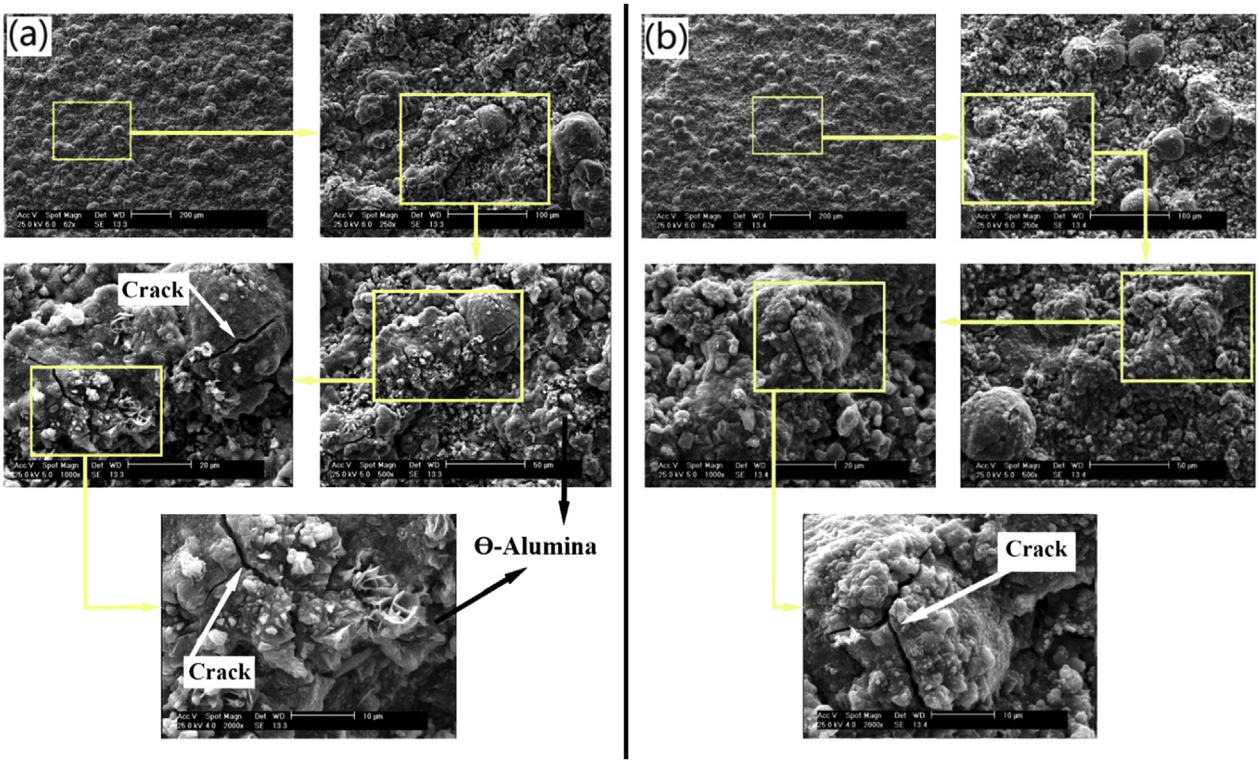

Fig. 10. Surface morphology of the (a) CoNiCrAlY and (b) NiCoCrAlY coating after 160 h oxidation.

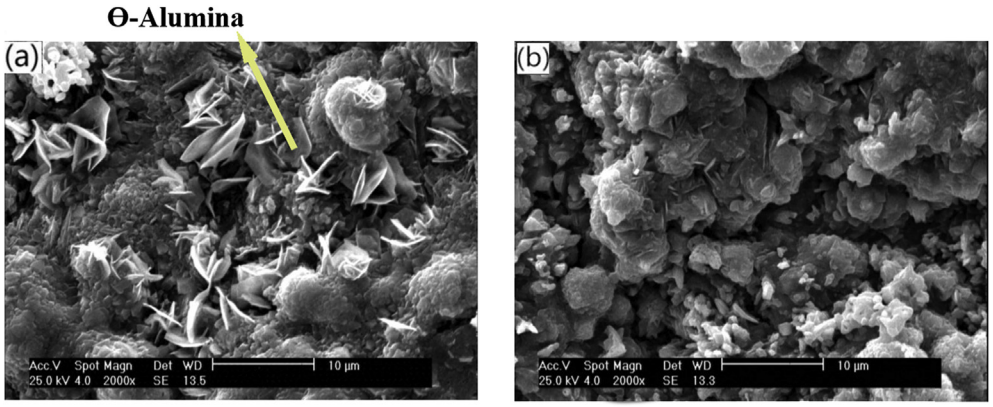

Fig. 11. Surface morphology of the (a) CoNiCrAlY and (b) NiCoCrAlY coating after 80 h oxidation.

As mentioned before when squared TGO thickness vs. time (squared specific mass-change vs. time) plot follows a linear relation, it means that the oxidation kinetic follows the parabolic law which is preferred in oxidation kinetic of coatings. It is obvious that having a linear plot of squared specific mass-change vs. time is somehow implausible practically. So it is necessary to find a parameter to check how much each plot is close to the linear preferable plot. To do this, the first step is to plot the best fit line through the points of the scatter plot.

The second step is to find the total deviation of the actual variables from the predicted values by the best fit line. The total amount of these deviations is called residuals that can be utilized to compare the oxidation kinetic behavior of different coatings. As some of the residuals are negative and some are positive, the sum of the square of the residuals is used. The following equation is utilized to find out the mentioned parameter. The best fit line and residual parameter can be obtained as shown in Fig. 14. The lower amount of the R parameter, the closer behavior to the parabolic law will be seen.

$$R = \sum_{i=1}^{i=n} \left(y_i - \left[\left[\left(\frac{\left(n \sum_{j=1}^{j=n} x_j y_j \right) - \left(\sum_{j=1}^{j=n} x_j \right) \left(\sum_{j=1}^{j=n} y_j \right)}{\left(n \sum_{j=1}^{j=n} x_j^2 \right) - \left(\sum_{j=1}^{j=n} x_j \right)^2} \right) (X_i) + \left(\frac{\left(\sum_{j=1}^{j=n} x_j^2 \right) \left(\sum_{j=1}^{j=n} y_j \right) - \left(\sum_{j=1}^{j=n} x_j \right) \left(\sum_{j=1}^{j=n} x_j y_j \right)}{\left(n \sum_{j=1}^{j=n} x_j^2 \right) - \left(\sum_{j=1}^{j=n} x_j \right)^2} \right) \right] \right]^2 \quad (8)$$

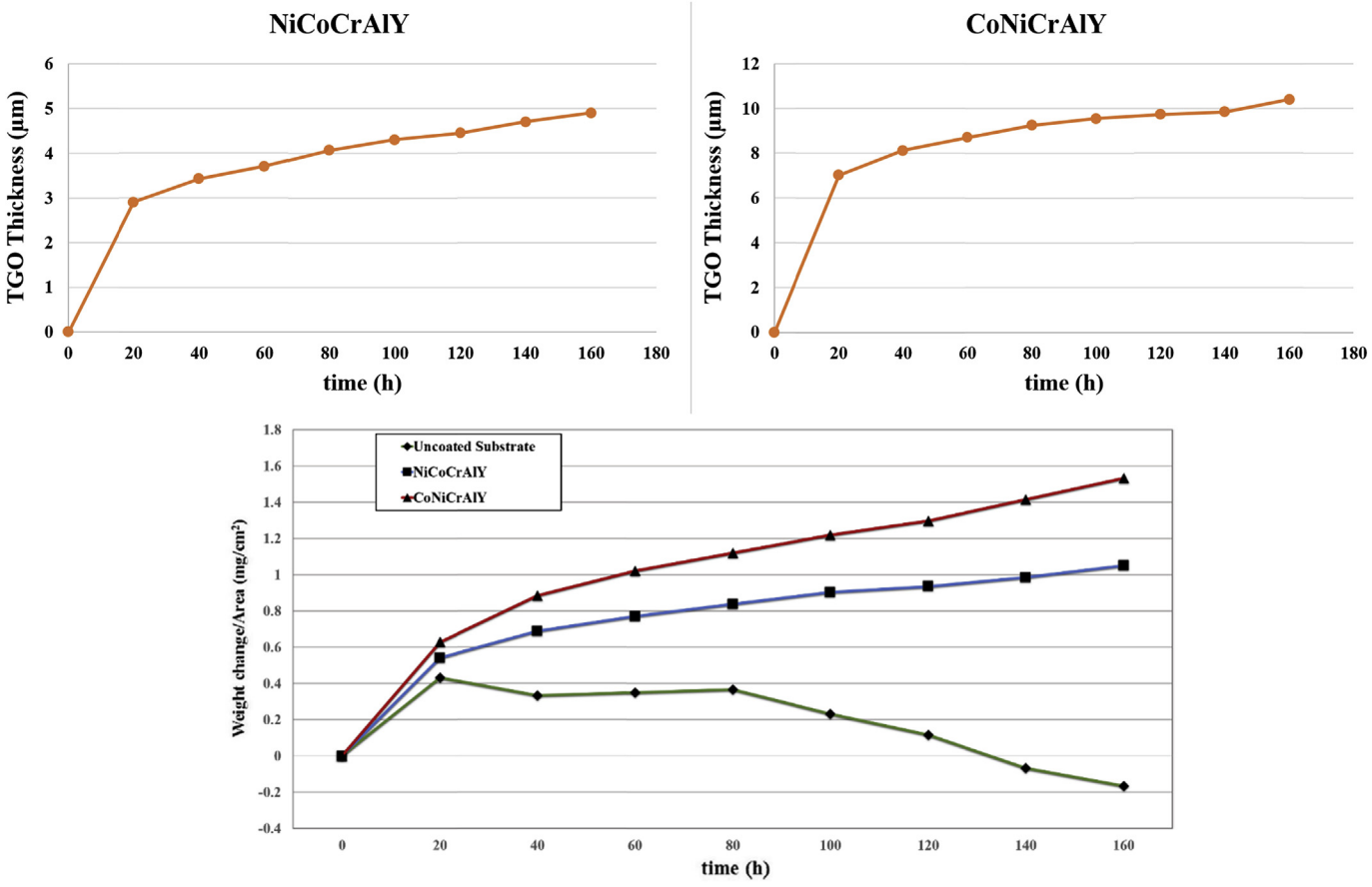

Fig. 12. TGO thickness and specific weight gain vs. time curves for both coated and bare substrate.

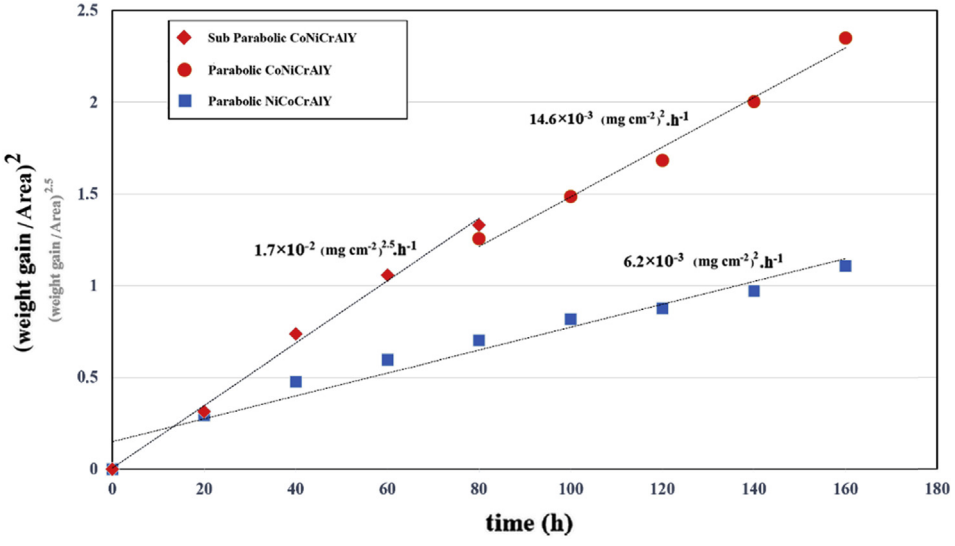

Fig. 13. Parabolic and sub-parabolic weight gain plots of the coatings during cyclic oxidation at 1000 °C.

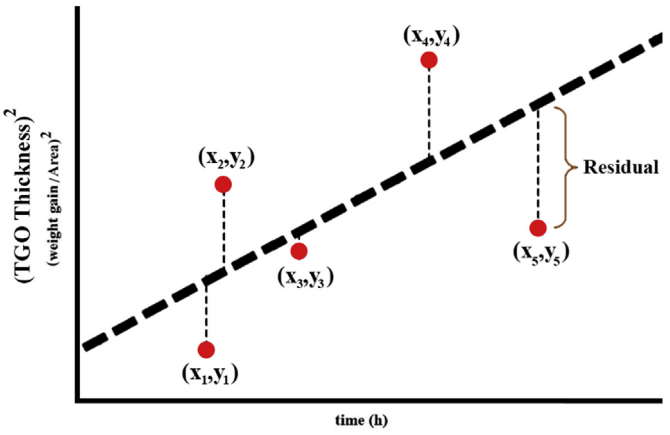

Fig. 14. Plotting the best fit line and residual in a sample scatter plot.

By using Equation (8), R parameter for NiCoCrAlY and CoNiCrAlY coatings were calculated 0.037 and 0.063 respectively based on TGO thickness procedure and 0.022 and 0.046 based on mass gain procedure. So it can be deduced that the NiCoCrAlY coating have better oxidation resistance because its oxidation kinetic curve has better parabolic behavior.

Comparing the ratio of the calculated rate constants based on different procedures, $(k_p^{CoNiCrAlY}/k_p^{NiCoCrAlY}) = 2.55$ and $(k_p^{'CoNiCrAlY}/k_p^{'NiCoCrAlY}) = 2.37$, demonstrate lower oxidation rate in the CoNiCrAlY coating based on the TGO thickness procedure. The main reason for the observed difference in these results is due to inner oxidation of the coatings, caused by some other parameters such as powder size, which can influence the mass change of the samples after each cycle. As in such a short time, 160 h, at the temperature of 1000 °C most of the MCrAlY coatings follow parabolic law, the sub parabolic behavior of the CoNiCrAlY coating in the first region may be caused by the internal oxidation of this coating too [28,45]. Using the TGO thickness may be a beneficial way for reducing these unwanted effects in obtaining the oxidation kinetic of coatings, instead of measuring the mass change.

4. Conclusions

The results of this study demonstrate that, unlike the NiCoCrAlY HVOF thermal sprayed coating which is covered with α-Alumina protective phase, the first oxide phase which forms on the CoNiCrAlY coating during high temperature cyclic oxidation at 1000 °C is θ-Alumina. The difference in coefficients of thermal expansion of CoNiCrAlY and θ-Alumina and, θ to α-Alumina conversion at higher oxidation time, impose high stress to the CoNiCrAlY coating and this transformation will cause high crack density in the CoNiCrAlY coating. Utilizing both TGO thickness and mass change of the coatings in calculating the rate constants of high temperature oxidation showed the higher resistance of NiCoCrAlY coating.

Acknowledgments

The authors would like to thank Iran National Science Foundation, Amirkabir University of Technology and Sharif University of Technology for their general support of the research.

References

[1] Y. Tamarin, Protective Coatings for Turbine Blades, ASM international, 2002.
[2] C. Duretthual, R. Morbioli, P. Steinmetz, Guide to the Control of High Temperature Corrosion and Protection of Gas Turbine Materials, 1986.
[3] W. Sloof, T. Nijdam, On the high-temperature oxidation of MCrAlY coatings, Int. J. Mater. Res. 100 (10) (2009) 1318–1330.
[4] J. Nicholls, Designing oxidation-resistant coatings, JoM 52 (1) (2000) 28.
[5] H. Yamano, K. Tani, Y. Harada, T. Teratani, Oxidation control with chromate pretreatment of MCrAlY unmelted particle and bond coat in thermal barrier systems, J. Therm. Spray Technol. 17 (2) (2008) 275–283.
[6] R.A. Miller, Thermal barrier coatings for aircraft engines: history and directions, J. Therm. Spray Technol. 6 (1) (1997) 35–42.
[7] S. Bose, High Temperature Coatings, Butterworth-Heinemann, 2011.
[8] W. Brandl, D. Toma, H. Grabke, The characteristics of alumina scales formed on HVOF-sprayed MCrAlY coatings, Surf. Coating. Technol. 108 (1998) 10–15.
[9] L. Pawlowski, The Science and Engineering of Thermal Spray Coatings, John Wiley & Sons, 2008.
[10] R. Taylor, J. Brandon, P. Morrell, Microstructure, composition and property relationships of plasma-sprayed thermal barrier coatings, Surf. Coating. Technol. 50 (2) (1992) 141–149.
[11] M. Di Ferdinando, A. Fossati, A. Lavacchi, U. Bardi, F. Borgioli, C. Borri, C. Giolli, A. Scrivani, Isothermal oxidation resistance comparison between air plasma sprayed, vacuum plasma sprayed and high velocity oxygen fuel sprayed CoNiCrAlY bond coats, Surf. Coating. Technol. 204 (15) (2010) 2499–2503.
[12] F. Yuan, Z. Chen, Z. Huang, Z. Wang, S. Zhu, Oxidation behavior of thermal barrier coatings with HVOF and detonation-sprayed NiCrAlY bondcoats, Corros. Sci. 50 (6) (2008) 1608–1617.
[13] F. Tang, L. Ajdelsztajn, G.E. Kim, V. Provenzano, J.M. Schoenung, Effects of surface oxidation during HVOF processing on the primary stage oxidation of a CoNiCrAlY coating, Surf. Coating. Technol. 185 (2) (2004) 228–233.
[14] Y. Itoh, M. Saitoh, Mechanical properties of overaluminized MCrAlY coatings at room temperature, Trans. ASME J. Eng. Gas Turbines Power 127 (4) (2005) 807.
[15] K. Ogawa, K. Ito, T. Shoji, D. Seo, H. Tezuka, H. Kato, Effects of Ce and Si additions to CoNiCrAlY bond coat materials on oxidation behavior and crack propagation of thermal barrier coatings, J. Therm. Spray Technol. 15 (4) (2006) 640–651.
[16] F. Tang, L. Ajdelsztajn, G.E. Kim, V. Provenzano, J.M. Schoenung, Effects of variations in coating materials and process conditions on the thermal cycle properties of NiCrAlY/YSZ thermal barrier coatings, Mater. Sci. Eng. A 425 (1–2) (2006) 94–106.
[17] G.-J. Yang, X.-D. Xiang, L.-K. Xing, D.-J. Li, C.-J. Li, C.-X. Li, Isothermal oxidation behavior of NiCoCrAlTaY coating deposited by high velocity air-fuel spraying, J. Therm. Spray Technol. 21 (3–4) (2012) 391–399.
[18] X. Liu, L. Huang, Z. Bao, X. Sun, H. Guan, Z. Hu, Preparation and cyclic oxidation of gradient NiCrAlYRe coatings on Ni-based superalloys, Surf. Coating. Technol. 202 (19) (2008) 4709–4713.
[19] H. Peng, H. Guo, J. He, S. Gong, Cyclic oxidation and diffusion barrier behaviors of oxides dispersed NiCoCrAlY coatings, J. Alloys Compd. 502 (2) (2010) 411–416.
[20] M. Daroonparvar, M.A.M. Yajid, N.M. Yusof, M.S. Hussain, H.R. Bakhsheshi-Rad, Formation of a dense and continuous Al 2 O 3 layer in nano thermal barrier coating systems for the suppression of spinel growth on the Al 2 O 3 oxide scale during oxidation, J. Alloys Compd. 571 (2013) 205–220.
[21] F. Pettit, Oxidation mechanisms for Ni-Al alloys at temperatures between 900 and 1300 C, AIME Met. Soc. Trans. 239 (9) (1967) 1296–1305.
[22] W. Chen, X. Wu, B. Marple, P. Patnaik, Oxidation and crack nucleation/growth in an air-plasma-sprayed thermal barrier coating with NiCrAlY bond coat, Surf. Coating. Technol. 197 (1) (2005) 109–115.
[23] T. Nijdam, W. Sloof, Modelling of composition and phase changes in multi-phase alloys due to growth of an oxide layer, Acta Mater. 56 (18) (2008) 4972–4983.
[24] N.P. Padture, M. Gell, E.H. Jordan, Thermal barrier coatings for gas-turbine engine applications, Science 296 (5566) (2002) 280–284.
[25] C. Giggins, F. Pettit, The oxidation of TD NiC (Ni-20Cr-2 vol pct ThO2) between 900° and 1200° C, Metall. Trans. 2 (4) (1971) 1071–1078.
[26] H. Evans, Stress effects in high temperature oxidation of metals, Int. Mater. Rev. 40 (1) (1995) 1–40.
[27] F. Tang, J.M. Schoenung, Local accumulation of thermally grown oxide in plasma-sprayed thermal barrier coatings with rough top-coat/bond-coat interfaces, Scripta Mater. 52 (9) (2005) 905–909.
[28] N. Birks, G.H. Meier, F.S. Pettit, Introduction to the High Temperature Oxidation of Metals, Cambridge University Press, 2006.
[29] H. Pei, Z. Wen, Y. Zhang, Z. Yue, Oxidation behavior and mechanism of a Ni-based single crystal superalloy with single α-Al 2 O 3 film at 1000° C, Appl. Surf. Sci. 411 (2017) 124–135.
[30] Doolabi, M.S., B. Ghasemi, S. Sadrnezhaad, A. Feizabadi, A. HabibollahZadeh, D.S. Doolabi, and M. AsadiZarch, Comparison of isothermal with cyclic oxidation behavior of "Cr-Aluminide" coating on inconel 738LC at 900° C. Oxid. Met.: p. 1-18.
[31] R. Prescott, M. Graham, The formation of aluminum oxide scales on high-temperature alloys, Oxid. Met. 38 (3–4) (1992) 233–254.
[32] Y. Han, F. Ye, G. Lu, C. Liu, L. Hao, Residual stress evolution of thermally grown oxide in thermal barrier coatings deposited onto nickel-base superalloy and iron-base alloy with thermal exposure ageing, J. Alloys Compd. 584 (2014) 19–27.
[33] J. Yang, E. Schumann, I. Levin, M. Rühle, Transient oxidation of NiAl, Acta Mater. 46 (6) (1998) 2195–2201.

[34] A. Feizabadi, M.S. Doolabi, S. Sadrnezhaad, H. Zafarani, D.S. Doolabi, M. AsadiZarch, MCDM selection of pulse parameters for best tribological performance of Cr–Al 2 O 3 nano-composite co-deposited from trivalent chromium bath, J. Alloys Compd. 727 (2017) 286–296.
[35] C. Xu, W. Gao, Pilling-Bedworth ratio for oxidation of alloys, Mater. Res. Innovat. 3 (4) (2000) 231–235.
[36] L. Ajdelsztajn, F. Tang, J. Schoenung, G.E. Kim, V. Provenzano, Synthesis and oxidation behavior of nanocrystalline MCrAlY bond coatings, J. Therm. Spray Technol. 14 (1) (2005) 23–30.
[37] H. Evans, R. Lobb, Conditions for the initiation of oxide-scale cracking and spallation, Corros. Sci. 24 (3) (1984) 209–222.
[38] K. Ma, J.M. Schoenung, Isothermal oxidation behavior of cryomilled NiCrAlY bond coat: homogeneity and growth rate of TGO, Surf. Coating. Technol. 205 (21) (2011) 5178–5185.
[39] K.M. Carling, E.A. Carter, Effects of segregating elements on the adhesive strength and structure of the α-Al 2 O 3/β-NiAl interface, Acta Mater. 55 (8) (2007) 2791–2803.
[40] M. Chen, M. Glynn, R. Ott, T. Hufnagel, K. Hemker, Characterization and modeling of a martensitic transformation in a platinum modified diffusion aluminide bond coat for thermal barrier coatings, Acta Mater. 51 (14) (2003) 4279–4294.
[41] D. Saber, I.S. Emam, R. Abdel-Karim, High temperature cyclic oxidation of Ni based superalloys at different temperatures in air, J. Alloys Compd. 719 (2017) 133–141.
[42] A. Rabiei, A. Evans, Failure mechanisms associated with the thermally grown oxide in plasma-sprayed thermal barrier coatings, Acta Materialia 48 (15) (2000) 3963–3976.
[43] C. Wagner, K. Grunewald, An article on the theory of the start-up procedure, Z. Phys. Chem. Abt. B 40 (1938) 455–475.
[44] C. Wagner, Theoretical analysis of the diffusion processes determining the oxidation rate of alloys, J. Electrochem. Soc. 99 (10) (1952) 369–380.
[45] S. Salam, P. Hou, Y.-D. Zhang, H.-F. Wang, C. Zhang, Z.-G. Yang, Compositional effects on the high-temperature oxidation lifetime of MCrAlY type coating alloys, Corros. Sci. 95 (2015) 143–151.